

# Observation of Feshbach resonances between alkali and closed-shell atoms

Vincent Barbé,<sup>1,\*</sup> Alessio Ciamei,<sup>1,\*</sup> Benjamin Pasquiou,<sup>1</sup> Lukas Reichsöllner,<sup>1</sup> Florian Schreck,<sup>1</sup> Piotr S. Żuchowski,<sup>2</sup> and Jeremy M. Hutson<sup>3</sup>

<sup>1</sup>*Van der Waals-Zeeman Institute, Institute of Physics, University of Amsterdam, Science Park 904, 1098XH Amsterdam, The Netherlands*

<sup>2</sup>*Institute of Physics, Faculty of Physics, Astronomy and Informatics, Nicolaus Copernicus University, ul. Grudziadzka 5/7, 87-100 Torun, Poland*

<sup>3</sup>*Joint Quantum Centre (JQC) Durham-Newcastle, Department of Chemistry, Durham University, South Road, Durham, DH1 3LE, United Kingdom*

(Dated: October 10, 2017)

Magnetic Feshbach resonances are an invaluable tool for controlling ultracold atoms and molecules [1]. They can be used to tune atomic interactions and have been used extensively to explore few- and many-body phenomena [2, 3]. They can also be used for magnetoassociation, in which pairs of atoms are converted into molecules by ramping an applied magnetic field across a resonance [4, 5]. Pairs of open-shell atoms, such as the alkalis, chromium [6], and some lanthanides [7–9], exhibit broad resonances because the corresponding molecule has multiple electronic states. However, molecules formed between alkali and closed-shell atoms have only one electronic state and no broad resonances. Narrow resonances have been predicted in such systems [10–12], but until now have eluded observation. Here we present the first observation of magnetic Feshbach resonances in a system containing a closed-shell atom, Sr, interacting with an alkali atom, Rb. These resonances pave the way to creating an ultracold gas of strongly polar, open-shell molecules, which will open up new possibilities for designing quantum many-body systems [13, 14] and for tests of fundamental symmetries [15].

A magnetic Feshbach resonance arises when a pair of ultracold atoms couples to a near-threshold molecular state that is tuned to be close in energy by an applied magnetic field. Magnetoassociation at such a resonance coherently transfers the atoms into the molecular state [16, 17]. In a few cases, near-threshold molecules formed in this way have been transferred to their absolute ground states [18–20], allowing exploration of quantum gases with strong dipolar interactions [21]. However, this has so far been achieved only for molecules formed from pairs of alkali atoms.

Mixtures of closed-shell alkaline-earth atoms with open-shell alkali atoms have been studied in several laboratories [22–25]. No strong coupling mechanism between atomic and molecular states exists in systems of this type, but theoretical work has identified weak coupling mech-

anisms that should lead to narrow Feshbach resonances, suitable for magnetoassociation [10–12]. In this letter we describe the detection of Feshbach resonances in mixtures of <sup>87</sup>Sr or <sup>88</sup>Sr with <sup>87</sup>Rb. The coupling between atomic and molecular states arises from two mechanisms previously predicted [10–12] and an additional, weaker mechanism that we identify here. The energies of the bound states responsible for the resonances are confirmed by two-photon photoassociation spectroscopy.

The experimental signature of a Feshbach resonance is field-dependent loss of Rb atoms. This may arise from either 3-body recombination or inelastic collisions, both of which are enhanced near a resonance. We perform loss spectroscopy using an ultracold Rb-Sr mixture, typically consisting of  $5 \times 10^4$  Rb atoms mixed with  $10^6$  <sup>87</sup>Sr or  $10^7$  <sup>88</sup>Sr atoms at a temperature of 2 to 5  $\mu$ K (see Methods). Figure 1 shows the observed loss features, eleven arising in the <sup>87</sup>Rb-<sup>87</sup>Sr Bose-Fermi mixture and one in the <sup>87</sup>Rb-<sup>88</sup>Sr Bose-Bose mixture. Ten loss features consist of a single, slightly asymmetrical dip with FWHM between 200 and 400 mG. The loss features labelled [1,0]a and [1,1]a each consist of several dips with a width of 20 to 60 mG at a spacing of 80 mG. We fit each dip with a Gaussian and give the resulting positions and widths in Tab. I. None of these Rb loss features arises in the absence of Sr, proving that they depend on Rb-Sr interactions. We also observe Rb loss features in the absence of Sr, which coincide with known Rb Feshbach resonances [26].

Both the atomic and molecular states are described by the total angular momentum of the Rb atom,  $f$ , and its projection  $m_f$  onto the magnetic field. Where necessary, atomic and molecular quantum numbers are distinguished with subscripts at and mol. In addition, the molecule has a vibrational quantum number  $n$ , counted down from  $n = -1$  for the uppermost level, and a rotational quantum number  $L$ , with projection  $M_L$ . <sup>88</sup>Sr has nuclear spin  $i_{\text{Sr}} = 0$ , whereas <sup>87</sup>Sr has  $i_{\text{Sr}} = 9/2$  and a corresponding projection  $m_{i,\text{Sr}}$ .

The near-threshold molecular states lie almost parallel to the Rb atomic states as a function of magnetic field. This is because the presence of the Sr atom barely changes the Rb hyperfine structure, and the Sr hyperfine energy is very small. We can therefore use the Breit-Rabi formula for Rb to convert the resonance posi-

\* RbSrFR@strontiumBEC.com;

These authors contributed equally to this work.

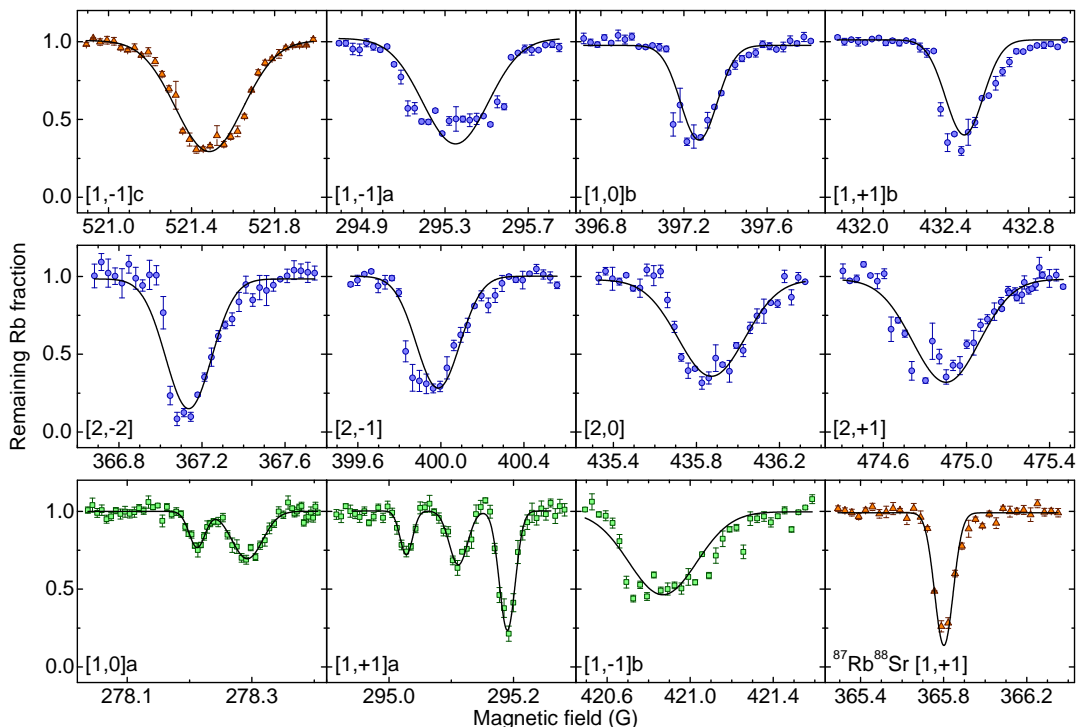


Figure 1. **Detection of Rb-Sr Feshbach resonances by field-dependent loss of Rb.** The fraction of Rb atoms remaining in state  $(f, m_f)$  after loss at each observed Feshbach resonance, normalised to unity far from the loss feature. Eleven loss features are observed in  $^{87}\text{Rb}$ - $^{87}\text{Sr}$  mixtures and one in  $^{87}\text{Rb}$ - $^{88}\text{Sr}$  (lower right panel). The loss features are labelled by  $[f, m_f]j$ , where  $j \in \{a, b, c\}$  is an index used when losses due to several molecular states are observed at the same atomic threshold. Most loss features show a single dip in the atom number, whereas  $[1,0]a$  and  $[1,+1]a$  show several. Each dip is fit by a Gaussian (black line), with results shown in Tab. I. The color and shape of symbols indicates the coupling mechanism for the Feshbach resonance: mechanism I (orange triangles), II (blue circles), or III (green squares). The resonance near 521 G also has a contribution from mechanism II. Error bars represent the standard error of three or more data points.

tions into zero-field binding energies  $E_b$  for the molecular states, which are given in Tab. II. The crossing atomic and molecular levels are shown in Figs. 2 and 3, with filled symbols where we observe loss features.

To verify the bound-state energies and validate our model of Feshbach resonances, we use two-photon photoassociation (PA) spectroscopy. We detect the two  $n = -2$  states (with  $L = 0$  and 2) below the lower ( $f = 1$ ) threshold of  $^{87}\text{Rb}$ - $^{87}\text{Sr}$  (states E and F in Tab. II) at almost exactly the energies deduced from the resonance positions. All the states observed through Feshbach resonances (B to F) also arise to within 2 MHz in a more complete model of the Rb-Sr interaction potential, as described below.

Three different coupling mechanisms are responsible for the observed loss features. The first mechanism was proposed in ref. [10] and relies on the change of the Rb hyperfine splitting when the Rb electron distribution is perturbed by an approaching Sr atom. Its coupling strength is proportional to the magnetic field in the field region explored here [12]. Since only states of equal  $m_f$  and  $L$  are coupled, it leads to Feshbach resonances only at crossings between atomic states with Rb in  $f = 1$  and molecular states with  $L = 0$  that correlate with  $f = 2$ . We observe

one such resonance with each of  $^{87}\text{Sr}$  and  $^{88}\text{Sr}$ .

The second mechanism involves hyperfine coupling of the Sr nucleus to the valence electron of Rb and was first proposed in ref. [11]. Since only fermionic  $^{87}\text{Sr}$  has a nuclear magnetic moment, this can occur only in Rb- $^{87}\text{Sr}$  collisions. This coupling conserves  $L$  and  $m_f + m_{i,\text{Sr}}$ , with the selection rule  $m_{f,\text{at}} - m_{f,\text{mol}} = 0, \pm 1$ . Crossings that fulfil these conditions occur also for molecular states with the same  $f$  value as the atomic state, which makes them much more abundant than crossings obeying the selection rules of the first mechanism. Feshbach resonances belonging to different  $m_{i,\text{Sr}}$  are slightly shifted with respect to one another because of the weak Zeeman effect on the Sr nucleus and the weak Sr hyperfine splitting. However, since the shift is only  $\sim 10$  mG for neighboring  $m_{i,\text{Sr}}$ , much smaller than the width of the loss features of typically 300 mG, we do not resolve this splitting.

The third mechanism is the anisotropic interaction of the electron spin with the nucleus of either Rb or fermionic Sr. This mechanism can couple the  $s$ -wave atomic state to molecules with rotational quantum number  $L = 2$ . As usual, the total angular momentum projection (now  $m_f + m_{i,\text{Sr}} + M_L$ ) is conserved. If the Sr nucleus is involved, an additional selection rule is  $\Delta m_f = \pm 1$ . By

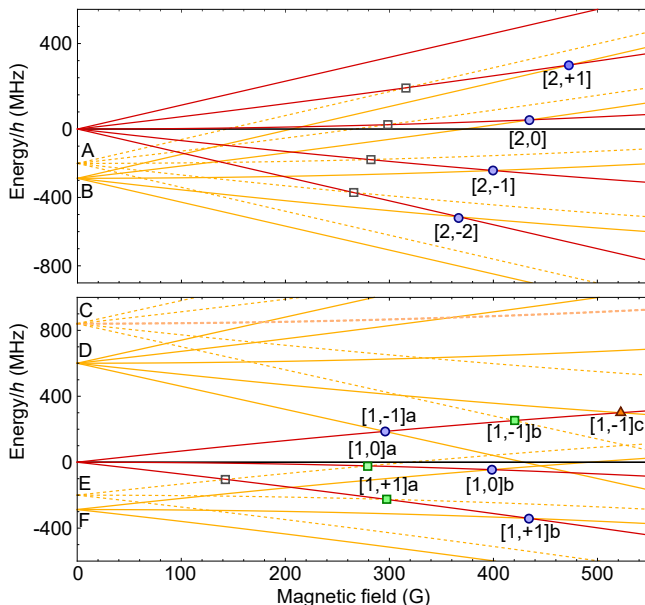


Figure 2. **Origin of the  $^{87}\text{Rb}$ - $^{87}\text{Sr}$  Feshbach resonances.** Energies of atomic (red) and molecular (orange) states as functions of magnetic field, shown with respect to the zero-field atomic level with  $f = 1$  or  $2$  as appropriate. Molecular states are labelled as in Tab. II and shown dashed if rotationally excited ( $L = 2$ ). Observed Feshbach resonances are labelled as in Fig. 1 and marked by filled symbols (orange triangles, blue circles or green squares for coupling mechanism I, II or III, respectively). Predicted but unobserved Feshbach resonances are marked by hollow symbols.

contrast, if the Rb nucleus is involved, the selection rule is  $\Delta m_f = -\Delta M_L$ . These loss features are made up of many  $(m_f, M_L)$  components, split by several hyperfine terms [27]; in some cases the components separate into groups for different values of  $M_L$ . Three loss features are attributed to this mechanism and two of them ([1,1]a and [1,0]a) indeed show a structure of two or three dips.

Table I includes a theoretical width  $\Delta$ , obtained from the Golden Rule approximation [12]. However, this is a physically different quantity from the experimental width  $\delta$ , and for narrow resonances there is no simple link between them. We have also searched for further resonances predicted by our model, marked by hollow symbols in Fig. 2, but did not observe them.

We have previously carried out electronic structure calculations of the RbSr ground-state potential [28]. We have used the binding energies from two-photon photoassociation, supplemented by the Feshbach resonance positions measured here, to determine a short-range correction to this potential [29]. This allows us to estimate that the interspecies scattering length of  $^{87}\text{Rb}$ - $^{87}\text{Sr}$  is  $a_{87,87} > 1600(+600, -450) a_0$  and that of  $^{87}\text{Rb}$ - $^{88}\text{Sr}$  is  $a_{87,88} = 170(20) a_0$ , where  $a_0$  is the Bohr radius. The large positive scattering length for  $^{87}\text{Rb}$ - $^{87}\text{Sr}$  will produce a molecular state with binding energy  $h \times 25(15)$  kHz, which would lead to Feshbach resonances

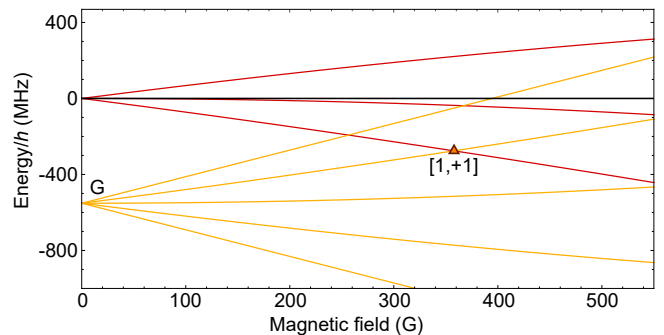


Figure 3. **Origin of the  $^{87}\text{Rb}$ - $^{88}\text{Sr}$  Feshbach resonance.** Energies of atomic (red) and molecular (orange) states as functions of magnetic field, shown with respect to the zero-field  $f = 1$  atomic level. Only one Feshbach resonance has been observed, produced by coupling mechanism I. Since  $^{88}\text{Sr}$  has zero nuclear spin, mechanism II is absent.

at low magnetic field. We searched for such resonances between 10 mG and 1 G, but did not find any.

There are several factors that affect resonance widths and hence observability. First, the amplitude of the atomic scattering function at short range depends on the background scattering length  $a$ ; it is largest when  $a$  is large, and the resonance widths are proportional to  $a$  in this regime [12]. This effect enhances all the resonance widths for  $^{87}\text{Rb}$ - $^{87}\text{Sr}$ . However, bound states very near dissociation exist mostly at long range, and the widths also depend on the binding energy as  $|E_b|^{2/3}$  [12]. This latter effect may explain our failure to observe the low-

Table I. **Properties of observed Feshbach resonances.** For resonances with many components, the theoretical width is the largest calculated value.

$[f, m_f]j$	(mol. state, $m_f, M_L$ )	$B$ (G)	$\delta$ (mG)	$\Delta$ (mG)	cpl. mech.
$^{87}\text{Rb}$ - $^{87}\text{Sr}$					
[2,+1]	(B, +2, 0)	474.9(4)	373(7)	0.04	II
[2,0]	(B, +1, 0)	435.9(4)	378(7)	0.07	II
[2,-1]	(B, 0, 0)	400.0(4)	247(4)	0.07	II
[2,-2]	(B, -1, 0)	367.1(4)	260(5)	0.04	II
[1,-1]a	(D, -2, 0)	295.4(4)	372(10)	0.33	II
[1,-1]b	(C, -2, mix)	420.9(4)	386(11)	0.002	III
[1,-1]c	(D, -1, 0)	521.5(4)	366(3)	2.4	I,II
[1,0]a	(E, -1, -1)	$B_1 = 278.2(4)$	30(3)	0.00009	III
	(E, -1, -2)	$B_1 + 0.081(2)$	58(4)	0.00011	III
[1,0]b	(F, -1, 0)	397.3(4)	207(4)	0.02	II
[1,+1]a	(E, 0, 0)	$B_2 = 295.0(4)$	24(3)	0.00002	III
	(E, 0, -1)	$B_2 + 0.083(2)$	35(3)	0.00009	III
	(E, 0, -2)	$B_2 + 0.162(2)$	30(1)	0.00011	III
[1,+1]b	(F, 0, 0)	432.5(4)	213(6)	0.02	II
$^{87}\text{Rb}$ - $^{88}\text{Sr}$					
[1,+1]	(G, +1, 0)	365.8(4)	105(2)	0.05	I

field resonances due to the state at  $E_b \approx h \times 25(15)$  kHz.

Our model enables us to predict the background scattering lengths and Feshbach resonance positions for all isotopic Rb-Sr mixtures [29]. For example, we predicted the position of the  $^{87}\text{Rb}$ - $^{88}\text{Sr}$  resonance after calibrating the model on  $^{87}\text{Rb}$ - $^{87}\text{Sr}$  Feshbach resonances and photoassociation results for three isotopic mixtures. This resonance was subsequently observed within 10 G of the prediction.

In summary, we have observed Feshbach resonances in mixtures of Rb alkali and Sr alkaline-earth atoms. Similar resonances will be ubiquitous in mixtures of alkali atoms with closed-shell atoms, particularly when the closed-shell atom has a nuclear spin. Magnetoassociation using resonances of this type offers a path towards a new class of ultracold molecules, with electron spin and strong electric dipole moment, which are expected to have important applications in quantum computation, many-body physics and tests of fundamental symmetries.

## ACKNOWLEDGMENTS

We thank the European Research Council (ERC) for funding under Project No. 615117 QuantStro. B.P. thanks the NWO for funding through Veni grant No. 680-47-438. P.S.Ż. thanks the Foundation for Polish Science for funding of Homing Plus project No. 2011-3/14 (co-financed by the EU European Regional Development Fund). J.M.H. thanks the UK Engineering and Physical Sciences Research Council for support under Grant No. EP/P01058X/1.

Table II. **Molecular states responsible for Feshbach resonances.** Binding energies obtained from observed Feshbach resonances,  $E_b^{\text{FR}}$ , and from two-photon photoassociation,  $E_b^{\text{PA}}$ .

label	$n$	$F$	$L$	$E_b^{\text{FR}}/h$ (MHz)	$E_b^{\text{PA}}/h$ (MHz)
$^{87}\text{Rb}$ - $^{87}\text{Sr}$					
A	-2	2	2	-	-
B	-2	2	0	288.2(4)	-
C	-4	2	2	5992(1)	-
D	-4	2	0	6234(1)	-
E	-2	1	2	200.0(3)	200.0(3)
F	-2	1	0	287.3(3)	287.3(2)
$^{87}\text{Rb}$ - $^{88}\text{Sr}$					
G	-4	2	0	7401.0(7)	-

## I. METHODS

**Sample preparation.** We prepare ultracold  $^{87}\text{Rb}$ - $^{87}\text{Sr}$  Bose-Fermi mixtures by methods similar to those in our previous work [30]. We transfer Rb and  $^{88}\text{Sr}$  from magneto-optical traps into a horizontal “reservoir” dipole trap with a waist of  $63(2)$   $\mu\text{m}$  and a wavelength of 1070 nm. After Rb laser cooling we optically pump Rb into the  $f = 1$  hyperfine state. By laser cooling Sr in the dipole trap on the narrow  $^1\text{S}_0$ - $^3\text{P}_1$  line we sympathetically cool Rb. We then transfer between  $5 \times 10^4$  and  $1 \times 10^5$  Rb atoms into the crossed-beam “science” dipole trap described below. We then ramp off the reservoir trap, discard  $^{88}\text{Sr}$  atoms and transfer between  $1 \times 10^6$  and  $2 \times 10^6$   $^{87}\text{Sr}$  atoms in a mixture of all ten nuclear spin states into the science trap. The final temperature is typically 2 to 5  $\mu\text{K}$ . In order to prepare Rb in an equal mixture of all three  $f = 1$   $m_f$  states we then randomize the distribution by non-adiabatic radiofrequency sweeps at a magnetic field of 130 G. To prepare Rb in the  $f = 2$  hyperfine states we instead use optical pumping, which directly produces a nearly homogeneous distribution of Rb over the  $f = 2$   $m_f$  states. To prepare  $^{87}\text{Rb}$ - $^{88}\text{Sr}$  Bose-Bose mixtures we do not discard  $^{88}\text{Sr}$  after transferring the gas into the science trap and we skip the loading of  $^{87}\text{Sr}$ .

**Science dipole trap.** The science trap consists of two copropagating horizontal beams and one vertical beam, all with coinciding foci. The first horizontal beam has a wavelength of 1064 nm and a waist of  $313(16)$   $\mu\text{m}$  ( $19(1)$   $\mu\text{m}$ ) in the horizontal (vertical) direction. The second horizontal beam has a wavelength of 532 nm and a waist of  $219(4)$   $\mu\text{m}$  ( $19(1)$   $\mu\text{m}$ ). The vertical beam has a wavelength of 1070 nm and a waist of  $78(2)$   $\mu\text{m}$ . The horizontal 1064-nm beam is typically used at a power of 5.7 W to 6.2 W and dominates the trap potential. The 532-nm beam is operated at 0.2 W to 0.4 W. The vertical beam is operated at 0.7(1) W to measure loss feature  $[1, -1]_b$  and is off otherwise. These operating conditions result in typical trap depths of  $40 \mu\text{K} \times k_B$  for Sr and  $95 \mu\text{K} \times k_B$  for Rb, taking account of gravitational sag.

**Loss spectroscopy.** We observe Feshbach resonances through field-dependent loss of Rb atoms. We submit the Rb-Sr mixture to a magnetic field of up to 550 G for a hold time of 1 to 10 s. Close to a Feshbach resonance, the rate of 2-body inelastic collisions or 3-body recombination is increased and atoms are lost. After the hold time we lower the magnetic field to near zero in 200 ms. During the next 10 ms, we ramp off the horizontal 532-nm beam and the vertical beam and decrease the power of the horizontal 1064-nm beam. This decrease lowers the evaporation threshold for Sr significantly, while Rb stays well trapped because its polarizability at 1064 nm is a factor of three higher. During the next 100 ms, Sr evaporates and cools Rb, which is advantageous for the subsequent imaging process.

At the end of the cooling stage, the science trap is switched off and a magnetic field gradient is applied to

perform Stern-Gerlach separation of the Rb  $m_f$  states. After 14 ms of expansion, absorption images of Sr and Rb are taken. To reduce sensitivity to Rb atom number fluctuations, we normalize the atom number of the Rb  $m_f$  state of interest by the total atom number in  $m_f$  states that are not lost. We verify that none of the loss features occurs in the absence of the Sr isotope concerned. For these verifications we need to retain a small amount of the other Sr isotope to allow sympathetic cooling.

**Adaptation of experimental conditions.** The width and depth of a loss feature depend on the measurement conditions. Thermal broadening sets a lower bound on the observable width, whereas hold time and peak densities affect the depth. For each resonance, we optimize the Sr density and hold time to maximize Rb loss without saturating the feature. We choose to use mixtures that contain much less Rb than Sr in order to obtain pronounced Rb loss features. Because of this atom number imbalance, and since most  $m_{i,\text{Sr}}$  states can contribute to a given loss feature, the fractional Sr loss during the hold time is small, which keeps the Rb loss rate high.

The resonances that we attribute to coupling mechanism II, with the exception of  $[1,-1]\text{a}$ , are recorded under identical conditions. The hold time is 5 s and the peak densities for Rb and  $^{87}\text{Sr}$  are  $2(1) \times 10^{11} \text{ cm}^{-3}$  and  $9(5) \times 10^{11} \text{ cm}^{-3}$ , respectively. The temperature of the Rb-Sr mixture before the hold time is  $4.5(5) \mu\text{K}$ .

The  $[1,-1]\text{a}$  and  $[1,-1]\text{c}$  resonances exhibit higher loss rates. For these we use hold times of 1.5 and 1 s, respectively. The peak densities for Rb and  $^{87}\text{Sr}$  are  $5(3) \times 10^{11} \text{ cm}^{-3}$  and  $2(1) \times 10^{12} \text{ cm}^{-3}$ . The temperature of the Rb-Sr mixture before the hold time is  $3.0(1) \mu\text{K}$ .

The resonances that we attribute to mechanism III exhibit much lower loss rates. Therefore we use a hold time of 10 s. To measure feature  $[1,-1]\text{b}$  we also add the vertical trapping beam to increase the gas densities. The peak densities for Rb are  $2(1) \times 10^{12} \text{ cm}^{-3}$ ,  $4(2) \times 10^{11} \text{ cm}^{-3}$  and  $3(2) \times 10^{11} \text{ cm}^{-3}$  for features  $[1,-1]\text{b}$ ,  $[1,0]\text{a}$  and  $[1,+1]\text{a}$  respectively. The peak densities for Sr are  $5(2) \times 10^{12} \text{ cm}^{-3}$ ,  $2(1) \times 10^{12} \text{ cm}^{-3}$  and  $4(2) \times 10^{12} \text{ cm}^{-3}$  respectively. The temperatures of the Rb-Sr mixture before the hold time are respectively  $5(1) \mu\text{K}$ ,  $3.2(2) \mu\text{K}$  and  $3.0(2) \mu\text{K}$ .

The  $[1,+1]$  resonance observed in the Rb- $^{88}\text{Sr}$  mixture exhibits a high loss rate, because we typically load one order of magnitude more  $^{88}\text{Sr}$  atoms than  $^{87}\text{Sr}$  atoms into the science trap due to the naturally higher abundance of  $^{88}\text{Sr}$ . We use a hold time of 1 s and we do not use the

532-nm trapping beam. The peak densities for Rb and  $^{88}\text{Sr}$  are  $6(3) \times 10^{11} \text{ cm}^{-3}$  and  $1.1(6) \times 10^{13} \text{ cm}^{-3}$ . The temperature of the Rb-Sr mixture before the hold time is  $2.2(1) \mu\text{K}$ .

**Magnetic field.** We use three pairs of coils to produce a homogeneous magnetic field across the atomic sample. The primary coils create a field up to  $\sim 500$  G with a resolution of 40 mG. These coils are used alone to record most of the loss features shown in Fig. 1. A second pair of coils is employed to resolve the substructure of the  $[1,0]\text{a}$  and  $[1,+1]\text{a}$  loss features, with the primary coils producing bias fields of 278 G and 294 G, respectively. The secondary coils create a low magnetic field with a resolution of 3 mG. A third pair of coils is used to supplement the primary coils to observe the  $[1,-1]\text{c}$  loss feature, creating a bias field of 57 G.

We calibrate the magnetic field produced by the primary coils up to 290 G by spectroscopy on the narrow  $^1\text{S}_0\text{-}^3\text{P}_1$  line of  $^{88}\text{Sr}$ . We use a current transducer (LEM IT 600-S) to interpolate between the calibration points and to extrapolate to higher fields. We calibrate the secondary coils by recording one of the three  $[1,+1]\text{a}$  loss features for different values of the field from the primary coils.

The magnetic field precision is limited by the resolution and noise of the power supplies. The inductances of the coils reduce the noise contribution to less than 40 mG from all three pairs of coils combined. The accuracy is limited mainly by drifts in the ambient magnetic field. Monitoring the position of the  $^{88}\text{Sr}$  MOT and the position of the loss feature due to a known Rb Feshbach resonance gives an upper bound of 350 mG for these drifts over the course of the present work. The calibration and statistical errors are typically one order of magnitude lower than the drifts. In addition, the positions of the loss maxima at finite temperature may differ from the positions of zero-energy Feshbach resonance positions. We account for this systematic error in the binding energies of Tab. II by adding an uncertainty of 4 times the root-mean-square width of the fitted Gaussian function.

## II. AUTHOR CONTRIBUTIONS

V.B., A.C. and L.R. performed the experiments. B.P. and F.S. supervised the experimental work. P.S.Ž. and J.M.H. contributed theoretical analysis. All authors were involved in analysis and discussions of the results and contributed to the preparation of the manuscript.

- 
- [1] C. Chin, R. Grimm, P. Julienne, and E. Tiesinga, “Feshbach resonances in ultracold gases,” *Rev. Mod. Phys.* **82**, 1225 (2010).  
 [2] C. H. Greene, P. Giannakeas, and J. Pérez-Ríos, “Universal few-body physics and cluster formation,” *Rev.*

*Mod. Phys.* **89**, 035006 (2017).

- [3] I. Bloch, J. Dalibard, and W. Zwerger, “Many-body physics with ultracold gases,” *Rev. Mod. Phys.* **80**, 885 (2008).

- [4] J. M. Hutson and P. Soldán, “Molecule formation in ultracold atomic gases,” *Int. Rev. Phys. Chem.* **25**, 497 (2006).
- [5] T. Köhler, K. Góral, and P. S. Julienne, “Production of cold molecules via magnetically tunable Feshbach resonances,” *Rev. Mod. Phys.* **78**, 1311 (2006).
- [6] J. Werner, A. Griesmaier, S. Hensler, J. Stuhler, T. Pfau, A. Simoni, and E. Tiesinga, “Observation of Feshbach resonances in an ultracold gas of  $^{52}\text{Cr}$ ,” *Phys. Rev. Lett.* **94**, 183201 (2005).
- [7] A. Frisch, M. Mark, K. Aikawa, F. Ferlaino, J. L. Bohn, C. Makrides, A. Petrov, and S. Kotochigova, “Quantum chaos in ultracold collisions of gas-phase erbium atoms,” *Nature* **507**, 475 (2014).
- [8] K. Baumann, N. Q. Burdick, M. Lu, and B. L. Lev, “Observation of low-field Fano-Feshbach resonances in ultracold gases of dysprosium,” *Phys. Rev. A* **89**, 020701 (2014).
- [9] S. Taie, S. Watanabe, T. Ichinose, and Y. Takahashi, “Feshbach-resonance-enhanced coherent atom-molecule conversion with ultranarrow photoassociation resonance,” *Phys. Rev. Lett.* **116**, 043202 (2016).
- [10] P. S. Żuchowski, J. Aldegunde, and J. M. Hutson, “Ultracold RbSr molecules can be formed by magnetoassociation,” *Phys. Rev. Lett.* **105**, 153201 (2010).
- [11] D. A. Brue and J. M. Hutson, “Magnetically tunable Feshbach resonances in ultracold Li-Yb mixtures,” *Phys. Rev. Lett.* **108**, 043201 (2012).
- [12] D. A. Brue and J. M. Hutson, “Prospects of forming ultracold molecules in  $^2\Sigma$  states by magnetoassociation of alkali-metal atoms with Yb,” *Phys. Rev. A* **87**, 052709 (2013).
- [13] A. Micheli, G. K. Brennen, and P. Zoller, “A toolbox for lattice-spin models with polar molecules,” *Nature Phys.* **2**, 341 (2006).
- [14] M. A. Baranov, M. Dalmonte, G. Pupillo, and P. Zoller, “Condensed matter theory of dipolar quantum gases,” *Chem. Rev.* **112**, 5012 (2012).
- [15] E. R. Meyer and J. L. Bohn, “Electron electric-dipole-moment searches based on alkali-metal- or alkaline-earth-metal-bearing molecules,” *Phys. Rev. A* **80**, 042508 (2009).
- [16] C. A. Regal, C. Ticknor, J. L. Bohn, and D. S. Jin, “Creation of ultracold molecules from a Fermi gas of atoms,” *Nature* **424**, 47 (2003).
- [17] J. Herbig, T. Kraemer, M. Mark, T. Weber, C. Chin, H. C. Nägerl, and R. Grimm, “Preparation of a pure molecular quantum gas,” *Science* **301**, 1510 (2003).
- [18] K.-K. Ni, S. Ospelkaus, M. H. G. de Miranda, A. Pe’er, B. Neyenhuis, J. J. Zirbel, S. Kotochigova, P. S. Julienne, D. S. Jin, and J. Ye, “A high phase-space-density gas of polar molecules in the rovibrational ground state,” *Science* **322**, 231 (2008).
- [19] J. G. Danzl, M. J. Mark, E. Haller, M. Gustavsson, R. Hart, J. Aldegunde, J. M. Hutson, and H.-C. Nägerl, “An ultracold, high-density sample of rovibronic ground-state molecules in an optical lattice,” *Nature Phys.* **6**, 265 (2010).
- [20] T. Takekoshi, L. Reichsöllner, A. Schindewolf, J. M. Hutson, C. R. Le Sueur, O. Dulieu, F. Ferlaino, R. Grimm, and H.-C. Nägerl, “Ultracold dense samples of dipolar RbCs molecules in the rovibrational and hyperfine ground state,” *Phys. Rev. Lett.* **113**, 205301 (2014).
- [21] S. A. Moses, J. P. Covey, M. T. Miecikowski, D. S. Jin, and J. Ye, “New frontiers for quantum gases of polar molecules,” *Nature Phys.* **13**, 13 (2017).
- [22] H. Hara, Y. Takasu, Y. Yamaoka, J. M. Doyle, and Y. Takahashi, “Quantum degenerate mixtures of alkali and alkaline-earth-like atoms,” *Phys. Rev. Lett.* **106**, 205304 (2011).
- [23] A. H. Hansen, A. Khramov, W. H. Dowd, A. O. Jamison, V. V. Ivanov, and S. Gupta, “Quantum degenerate mixture of ytterbium and lithium atoms,” *Phys. Rev. A* **84**, 011606 (2011).
- [24] M. Borkowski, P. S. Żuchowski, R. Ciuryło, P. S. Julienne, D. Kędziera, L. Mentel, P. Tecmer, F. Münchow, C. Bruni, and A. Görlitz, “Scattering lengths in isotopologues of the RbYb system,” *Phys. Rev. A* **88**, 052708 (2013).
- [25] A. Guttridge, S. A. Hopkins, S. L. Kemp, M. D. Frye, J. M. Hutson, and S. L. Cornish, “Interspecies thermalization in an ultracold mixture of Cs and Yb in an optical trap,” *Phys. Rev. A* **96**, 012704 (2017).
- [26] A. Marte, T. Volz, J. Schuster, S. Dürr, G. Rempe, E. G. M. van Kempen, and B. J. Verhaar, “Feshbach resonances in rubidium 87: Precision measurement and analysis,” *Phys. Rev. Lett.* **89**, 283202 (2002).
- [27] J. Aldegunde and J. M. Hutson, “Hyperfine structure of  $^2\Sigma$  molecules containing alkaline-earth atoms” (2017).
- [28] P. S. Żuchowski, R. Guérout, and O. Dulieu, “Ground- and excited-state properties of the polar and paramagnetic RbSr molecule: A comparative study,” *Phys. Rev. A* **90**, 012507 (2014).
- [29] A. Ciamei, *et al.*, in preparation.
- [30] B. Pasquiou, A. Bayerle, S. M. Tzanova, S. Stellmer, J. Szczepkowski, M. Parigger, R. Grimm, and F. Schreck, “Quantum degenerate mixtures of strontium and rubidium atoms,” *Phys. Rev. A* **88**, 023601 (2013).